Int J Adv Manuf Technol
DOI 10.1007/s00170-015-7764-0

ORIGINAL ARTICLE

Optimization of AISI 1045 end milling using robust parameter design

T. G. Brito[1] · A. P. Paiva[1] · T. I. Paula[1] · D. N. Dalosto[1] · J. R. Ferreira[1] · P. P. Balestrassi[1]

Received: 10 March 2015 / Accepted: 27 August 2015

Abstract AISI 1045 steel end milling, which enables manufacturers to machine parts with low-cost tools, has been gaining prominence in the industry. To ensure the quality of the final products though, it is important to properly adjust the process parameters so as to avoid premature tool wear while providing good levels of productivity along with zero defects. This study aims to optimize the end milling of AISI 1045 steel, using carbide inserts coated with titanium nitride (TIN). The objective—to produce the best surface finishing for machined parts—is achieved by identifying the optimal combination of input parameters and output variables. While the responses analyzed consist of surface roughness, Ra and Rt, the study also considers how Ra and Rt are impacted by the cutting fluid and tool wear during the process. The process parameters analyzed include cutting speed (vc), feed per tooth (fz), axial depth of cut (ap), and radial depth (ae). The noise variables considered are tool wear (z_1), cutting fluid concentration (z_2), and flow rate (z_3). To obtain optimal results, 82 experiments of a combined response surface array are conducted to collect data and analyze the effects of the parameters. In such a design, noise factors are used to generate variation for the responses, allowing the estimation of a mean and a variance equation for Ra and Rt. To optimize the process, a weighted mean square error (MSE) approach is used to form a set of optimal and non-dominated solutions through a Pareto frontier. In this manner, depending on the weight assigned to the mean or variance equation, the algorithm leads to a feasible solution. Theoretical and practical results obtained confirm the adequacy of this proposal; a minimal surface roughness is achieved with the smallest possible influence from tool wear, cutting fluid concentration, and flow rate.

Keywords End milling · Robust parameter design (RPD) · Response surface methodology (RSM) · Mean square error (MSE) · Optimization

✉ P. P. Balestrassi
pedro@unifei.edu.br

[1] Institute of Industrial Engineering and Management, Federal University of Itajuba, Itajuba, Minas Gerais, Brazil

1 Introduction

Among the various machining processes adopted in real manufacturing environments, one of the most fundamental and commonly encountered for material removal operations is the end milling process. In the end milling process, an important property in the evaluation of workpiece quality is the surface roughness [1–8]. Although there is a great deal of research on surface roughness modeling and predicting this kind of process [1–8], few efforts have been made at assessing the influence of noise factors on end milling process performance.

An alternative strategy used to make such an assessment involves design of experiments (DOE) and, in particular, robust parameter design (RPD) [9, 10]. RPD was developed to promote the best levels of control factors capable of making processes less sensitive to the actions of noise variables, of improving the variability control, and of minimizing the bias [11]. The RDP presented in this work facilitates the adaptive control application in the end milling process and contributes to computer-integrated manufacturing designs [11–13]. Originally developed following a crossed-array [10], RPD remains controversial. The controversy springs from the mathematical flaws and statistical inconsistencies stemming from the inability of crossed arrays to assess the interaction between control and noise variables [12–15].

Published online: 12 September 2015

The main drawback of crossed arrays is the excessive number of experiments needed [10]. To surmount this obstacle, Vining and Myers [9] and Box and Jones [10] proposed the use of response surface methodology (RSM) with combined arrays [14–17]. This experimental strategy allows the computation of noise-control interactions using a central composite design (CCD) with embedded noise factors, generating the mean and variance equation from the propagation-of-error principle [11–14]. The general scheme of working out an RPD-RSM problem consists of performing a CCD design with the noise factors considered as control variables and eliminating the axial points related to the noise factors from the design [10]. Using an OLS or a WLS algorithm, a polynomial surface for $f(\mathbf{x}, \mathbf{z})$ is estimated. Taking its partial derivatives in terms of the noise factors, the response surfaces for the mean $\hat{y}(\mathbf{x})$ and variance $\hat{\sigma}^2(\mathbf{x})$ are determined [14].

In terms of optimization, mean $\hat{y}(\mathbf{x})$ and variance $\hat{\sigma}^2(\mathbf{x})$ may be treated as two objective functions that may be joined into a global objective function F($\mathbf{x}$) using a weighted sum [12–25]. It is also possible to use the square deviation between the mean and the target proposed for the objective function. In both approaches, the global objective function must be minimized. This global objective function is known as mean square error (MSE) [20, 22–24]. Assuming that mean and variance may be assigned different degrees of importance, MSE becomes $F(\mathbf{x})=w[\mu(\mathbf{x})-T_y]^2+(1-w)\sigma^2(\mathbf{x}), 0\leq w\leq 1$. This objective function may be subjected to any constraint g($\mathbf{x}$)≤0. However, since a CCD is used to estimate the objective functions, a common choice for the constraint is the spherical region in which the experiment was done, such as $g(\mathbf{x})=\mathbf{x}^T\mathbf{x}\leq\alpha^2$ [24]. Minimizing the MSE ensures that the average response is established as close as possible to its target, while presenting minimal variability. Such optimization may be written as follows [20–24]:

$$\begin{aligned}&\underset{x\in\Omega}{\text{Minimize}} && F(\mathbf{x}) = w\left[\hat{\mu}(\mathbf{x})-T_y\right]^2 + (1-w)\hat{\sigma}^2(\mathbf{x})\\ &\text{Subject to :} && \mathrm{g}(\mathbf{x}) = \mathbf{x}^T\mathbf{x}\leq\alpha^2\end{aligned} \tag{1}$$

where F($\mathbf{x}$) is the MSE of the response y($\mathbf{x}$,$\mathbf{z}$), $\hat{\mu}(\mathbf{x})$ and $\hat{\sigma}^2(\mathbf{x})$ are the mean and variance models for y($\mathbf{x}$,$\mathbf{z}$), T_y is the target of response y($\mathbf{x}$,$\mathbf{z}$), and $\mathbf{x}^T\mathbf{x}\leq\alpha^2$ is a spherical nonlinear constraint denoting the experimental space.

2 Multi-response robust parameter optimization based on combined arrays

A robust response surface model is a polynomial that involves linear interactions and quadratic terms promoted by the variation of control parameters. This is in addition to the consideration of noise effects and their interactions with the control parameters, the effects of which may be estimated using a combined array [11–13]. The general model may be written as Eq. (2):

$$\begin{aligned}y(\mathbf{x},\mathbf{z}) = \beta_0 + \sum_{i=1}^{k}\beta_i x_i + \sum_{i=1}^{k}\beta_{ii}x_i^2 + \sum_{i<j}\sum\beta_{ij}x_i x_j\\ + \sum_{i=1}^{k}\gamma_i z_i + \sum_{i=1}^{k}\sum_{j=1}^{r}\delta_{ij}x_i z_j + \varepsilon\end{aligned} \tag{2}$$

Assuming that noise variables are independent with zero mean and variances σ_z^2 and the random error are uncorrelated, the mean and variance models can be written as Eqs. (3) and (4):

$$E_z[y(\mathbf{x},\mathbf{z})] = f(\mathbf{x}) \tag{3}$$

$$V_z[y(\mathbf{x},\mathbf{z})] = \sigma_{z_i}^2\left\{\sum_{i=1}^{r}\left[\frac{\partial y(\mathbf{x},\mathbf{z})}{\partial z_i}\right]^2\right\} + \sigma^2 \tag{4}$$

where k and r are the numbers of control and noise variables, respectively.

In Eq. (4), $\sigma_{z_i}^2$ is equal to 1 and σ^2 is within the variation from an ANOVA of the full quadratic model of $\hat{y}(\mathbf{x},\mathbf{z})$. Note, however, that σ^2 is a constant and cannot be reduced by the optimization routine since it is independent of control and noise parameters. Replacing the mean and variance functions by their respective estimates obtained with the combined array and neglecting the variance term σ^2, the RPD problem may be written as a multi-objective optimization such as the following:

$$\begin{aligned}&\underset{x\in\Omega}{\text{Minimize}} && F(\mathbf{x}) = w\left\{E_z[y(\mathbf{x},\mathbf{z})]-T_y\right\}^2\\ & && + (1-w)\left[\sigma_{z_i}^2\left\{\sum_{i=1}^{r}\left[\frac{\partial y(\mathbf{x},\mathbf{z})}{\partial z_i}\right]^2\right\}\right]\\ &\text{Subject to :} && \mathrm{g}(\mathbf{x}) = \mathbf{x}^T\mathbf{x}\leq\alpha^2\end{aligned} \tag{5}$$

The solution of a multi-objective optimization problem is usually associated with a Pareto frontier [26]. A Pareto frontier is a set of solutions in which an improvement in one objective can exist only if there is a worsening in at least one of the other objectives. Therefore, each point of this border represents a feasible solution. Hence, for any given pair of solutions, such as vectors of values of the objective function, an improvement in one of its components involves a worsening in another. The Pareto frontier is built using the anchor points that define the extremes of the border. The anchor points are obtained when each objective is minimized independently and the line of utopia, which describes the line connecting two extreme anchor points in bi-objective cases and, in multi-objective cases, a plan that includes all the anchor points (hyperplane of utopia).

It is important to note that a problem is considered multi-objective convex if the feasible set X and functions are individual convex as well [27]. It is known that the set of feasible solutions of a convex multi-objective problem is also convex and that the Pareto frontier results in a convex curve. When group X is not feasibly convex, or at least one of the functions is not convex, the problem is considered not convex.

3 Numerical illustration

To accomplish its objective, this study carried out a set of 82 experiments on the end milling operation of AISI 1045 steel (Fig. 1a). The tool used was a positive end mill, code R390-025A25-11M with a 25-mm diameter, an entering angle of χ_r=90°, and a medium step (Sandvik-Coromant). Three rectangular inserts were used (Fig. 2b) with an edge length of 11 mm each, code R390-11T308M-PM GC 1025 (Sandvik-Coromant) with a tool overhang of 60 mm. The tool material used was cemented carbide ISO P10 coated by the PVD process with TiCN and TiN. The coating hardness was around 3000 HV3 and the substrate hardness 1650 HV3 with a grain size smaller than 1 μm. The workpiece material was AISI 1045 steel with a hardness of approximately 180 HB. The workpiece dimensions were rectangular blocks with a 100×100-mm square section and a length of 300 mm. All the milling experiments were carried out in a FADAL vertical machining center, model VMC 15, with maximum spindle rotation of 7500 rpm and 15 kW of power in the main motor. Following the experimental sequence of a combined array, the researchers designed a CCD with k=7 variables (x_1, x_2, x_3, x_4, z_1, z_2, and z_3) and ten center points, deleting the axial points related to the noise variables. Described in Tables 1 and 2 are the control and noise factors and respective adopted levels.

The different noise conditions, furnished by a combination of factors and levels described in Table 2, express in some sense the possible variations that could occur during the end milling operation. Such variations include tool flank wear (z_1), cutting fluid concentration (z_2), and cutting fluid flow rate (z_3). The cutting fluid used in the experiments was synthetic oil Quimatic MEII. The surface roughness values are expected to suffer some kind of variation due to the action of the combined noise factors. Therefore, the main objective of robust parameter design (RPD) is to find the control parameter setup capable of achieving a reduced surface roughness with minimal variance, while mitigating the influence of noise factors over the process performance.

The measurements of the tool flank wear (Vb) (z_1) were taken with an optical microscope (×40) using images acquired by a coupled digital camera. The criteria adopted as the end of tool life was a flank wear of approximately Vb=0.30 mm, as shown in Fig. 2b.

The responses measured in the end milling process were the arithmetic average surface roughness (Ra) and the maximum roughness height (Rt) (distance from highest peak to lowest valley). In this work, both surface roughness metrics were assessed using a Mitutoyo portable roughness meter, model Surftest SJ 201, with a cutoff length of 0.8 mm (Fig. 1c).

This procedure resulted in 82 experiments, described in Table 3. The two surface roughness metrics were measured three times each, with each being in a different position of the workpiece. The mean was computed after nine measurements.

4 Results and discussion

According to the discussion in Sect. 1, the mean and variance models developed using the combined array were written only in terms of control variables, although during the experimentation, the noise factors were used. However, given that the

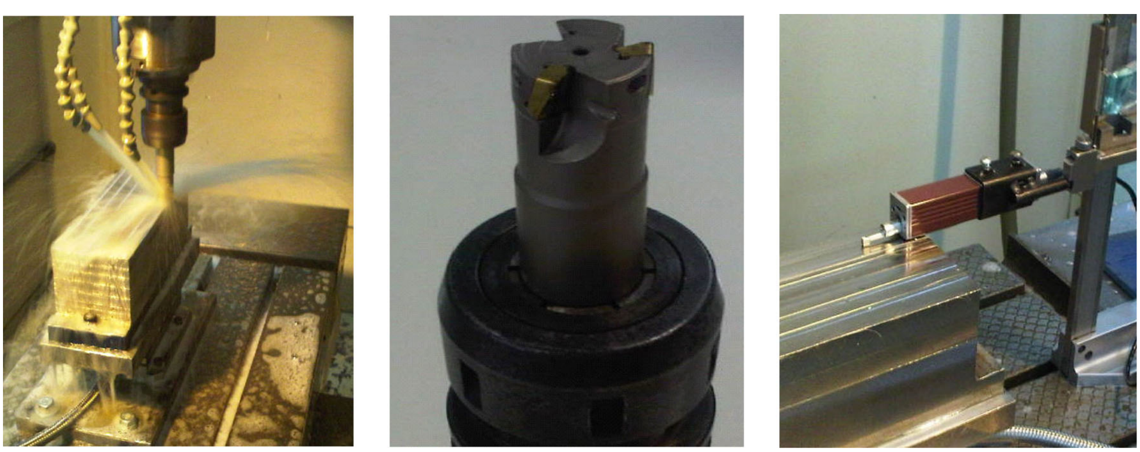

(a) (b) (c)

Fig. 1 **a** End milling process. **b** End milling tool. **c** Surface roughness measure

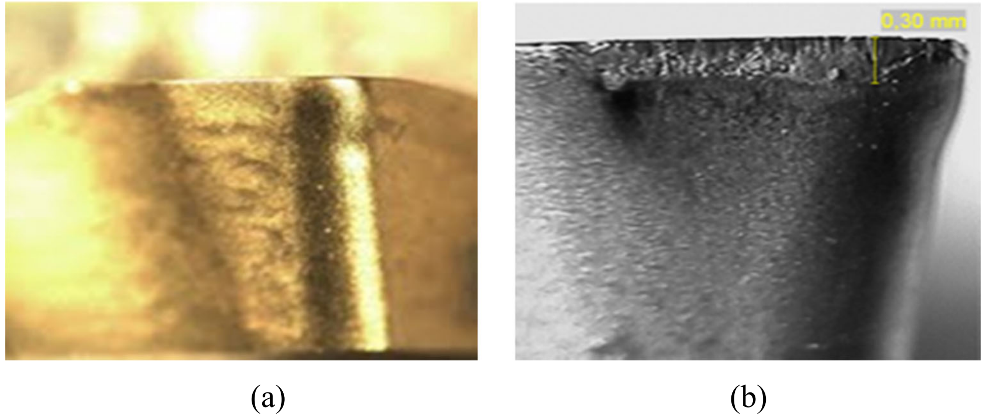

Fig. 2 **a** New tool. **b** Worn tool (Vb_{max}=0.30 mm)

variance equation takes into account the noise influence, the adjustment of the control factors leads to a minimization of process variability, ensuring the robustness of the end milling process.

Figure 3 shows that most of the interactions between input parameters were significant, representing an expressive nonlinearity in the surface roughness models.

According to these graphs, when both axial and radial depths of cut are increased, the average surface roughness (Ra) increases significantly. However, such a response surface is concave, suggesting that the minimal values for average surface roughness are obtained near the center point. A similar behavior is observed with the interaction between feed per tooth and axial depth of cut. Increasing both variables promotes higher values of Ra. The same effect is observed between feed per tooth and cutting speeds as well as feed per tooth and radial depth of cut. Such behaviors were expected. After all, the increment in cutting parameter levels significantly increases the vibration in the shaft, which increases the grooves made on the machined surface. The high-speed cutting with increased feed per tooth made the tool touch the sharp edge of the piece; early in the cut, the process was already at a disadvantage. When the radial depth of cut is increased and the cutting speed decreased, the insert moves with the least speed. This forces more plastic deformation and roughness damage. While the interaction effect on Rt behavior is similar to that on Ra, they are not identical; the average values (Ra) do not necessarily imply maximum peaks and valleys (Fig. 4).

One of the most important contributions of a combined array is the possibility of measuring the interaction effects between control and noise parameters. Though it is impossible to control the behavior of noise factors, an optimization algorithm may neutralize their influence by adjusting the levels of control factors. Figure 5 shows the most significant interactions of control and noise factors. It may be observed that for high values of feed per tooth, the average surface roughness will be larger with a worn-out tool than with a new tool. It may also be noted that the average surface roughness (Ra) is less with a new cutting edge than with a worn-out cutting edge. This effect is the opposite for small feed rate values.

So, depending on the flank wear level, the surface roughness will vary significantly along the range of feed rates. Figure 6 shows that the most prominent noise-control interaction in Rt is between axial depth of cut and flank tool wear. Figures 5 and 6 highlight that noise-control interactions are very important in modeling the expected values of surface roughness properly mainly because they influence the average values that promote a large prediction variance. Since these interactions are significant, the variance equations—dependent only on control factors—will correctly model the interference promoted by the noise factors; then, the minimization of variance equation will lead to a steady-state process.

The introduction of noise factors in the design of control factors generally causes an instability in the response surface model, reducing R^2 (Adj.) and increasing the MSE. To avoid such influence, the weighted least squares method (WLS) can be used. Applying the WLS method to estimate the coefficients of the response surfaces for Ra and Rt, the following models are obtained:

Table 1 Control factors and respective levels

Parameters	Unit	Symbol	Levels				
			−2.828	−1	0	+1	+2.828
Feed rate	mm/tooth	fz	0.010	0.100	0.150	0.200	0.290
Axial depth of cut	mm	ap	0.064	0.750	1.125	1.500	2.186
Cutting speed	m/min	vc	254	300	325	350	396
Radial depth of cut	mm	ae	12.260	15.000	16.500	18.000	20.740

Table 2 Noise factors and respective levels

Noise factors	Unit	Symbol	Levels		
			−1	0	+1
Flank tool wear	Mm	z_1	0.000	0.150	0.300
Cutting fluid concentration	%	z_2	5	10	15
Cutting fluid flow rate	l/min	z_3	0	10	20

$$
\begin{aligned}
\mathrm{Ra}(x,z) = {} & 0.689 + 0.898x_1 + 0.041x_1 - 0.006x_3 - 0.004x_4 \\
& + 0.102z_1 + 0.002z_2 + 0.005z_3 + 0.493x_1^2 \\
& + 0.096x_2^2 + 0.010x_3^2 + 0.064x_4^2 \\
& + 0.074x_1x_2 - 0.087x_1x_3 + 0.030x_1x_4 \\
& + 0.048x_1z_1 - 0.086x_1z_2 + 0.042x_1z_3 + 0.039x_2x_3 \\
& + 0.018x_2x_4 + 0.013x_2z_1 - 0.073x_2z_2 - 0.012x_2z_3 \\
& + 0.043x_3x_4 + 0.020x_3z_1 - 0.034x_3z_2 \\
& + -0.041x_3z_3 - 0.052x_4z_1 - 0.013x_4z_2 - 0.025x_4z_3
\end{aligned} \tag{5}
$$

$$
\begin{aligned}
\mathrm{Rt}(x,z) = {} & 4.719 + 3.170x_1 + 0.251x_2 - 0.261x_3 + 0.046x_4 \\
& + 0.877z_1 + 0.040z_2 - 0.049z_3 + 1.039x_1^2 \\
& + 0.176x_2^2 + 0.173x_4^2 + 0.498x_1x_2 - 0.225x_1x_3 \\
& + 0.233x_1x_4 + 0.310x_1z_1 - 0.291x_1z_2 \\
& + 0.188x_1z_3 - 0.020x_2x_3 + 0.164x_2x_4 - 0.087x_2z_1 \\
& + -0.210x_2z_2 - 0.127x_2z_3 + 0.181x_3x_4 \\
& + 0.128x_3z_1 - 0.109x_3z_2 + 0.042x_3z_3 \\
& + -0.158x_4z_1 - 0.016x_4z_2 + 0.157x_4z_3
\end{aligned} \tag{6}
$$

Employing the propagation-of-error principle and taking the partial derivatives of Eqs. (3) and (4), the respective mean and variance equations can be written as follows:

$$
\begin{aligned}
E_z[\mathrm{Ra}(\mathbf{x},\mathbf{z})] = {} & 0.689 + 0.898x_1 + 0.041x_2 - 0.06]6x_3 - 0.004x_4 \\
& + +0.493x_1^2 + 0.096x_2^2 + 0.010x_3^2 + 0.064x_4^2 \\
& + 0.074x_1x_2 + -0.087x_1x_3 \\
& + \ 0.030x_1x_4 - 0.039x_2x_3 + 0.018x_2x_4 \\
& + \ 0.043x_3x_4
\end{aligned} \tag{7}
$$

$$
\begin{aligned}
V_z[\mathrm{Ra}(\mathbf{x},\mathbf{z})] = {} & \left[\frac{\partial \mathrm{Ra}(\mathbf{x},\mathbf{z})}{\partial z_1}\right]^2 + \left[\frac{\partial \mathrm{Ra}(\mathbf{x},\mathbf{z})}{\partial z_2}\right]^2 \\
& + \left[\frac{\partial \mathrm{Ra}(\mathbf{x},\mathbf{z})}{\partial z_3}\right]^2 + \sigma^2
\end{aligned} \tag{8}
$$

Table 3 Experimental design

Run	fz	ap	vc	ae	z_1	z_2	z_3	Ra	Rt
(Part I)									
1	0.100	0.750	300	15.000	0.000	5	20	0.297	2.097
2	0.200	0.750	300	15.000	0.000	5	0	1.807	7.587
3	0.100	1.500	300	15.000	0.000	5	0	0.657	3.467
4	0.200	1.500	300	15.000	0.000	5	20	2.573	8.957
5	0.100	0.750	350	15.000	0.000	5	0	0.353	2.160
6	0.200	0.750	350	15.000	0.000	5	20	3.013	9.327
7	0.100	1.500	350	15.000	0.000	5	20	0.270	1.973
8	0.200	1.500	350	15.000	0.000	5	0	2.417	8.743
9	0.100	0.750	300	18.000	0.000	5	0	0.320	2.087
10	0.200	0.750	300	18.000	0.000	5	20	3.170	11.583
11	0.100	1.500	300	18.000	0.000	5	20	0.280	1.690
12	0.200	1.500	300	18.000	0.000	5	0	2.877	10.187
13	0.100	0.750	350	18.000	0.000	5	20	0.270	2.027
14	0.200	0.750	350	18.000	0.000	5	0	3.030	11.197
15	0.100	1.500	350	18.000	0.000	5	0	0.550	3.340
16	0.200	1.500	350	18.000	0.000	5	20	1.520	7.043
17	0.100	0.750	300	15.000	0.300	5	0	0.497	4.560
18	0.200	0.750	300	15.000	0.300	5	20	2.770	10.973
19	0.100	1.500	300	15.000	0.300	5	20	0.383	2.707
20	0.200	1.500	300	15.000	0.300	5	0	3.247	12.473
21	0.100	0.750	350	15.000	0.300	5	20	0.760	4.647
22	0.200	0.750	350	15.000	0.300	5	0	0.800	4.580
23	0.100	1.500	350	15.000	0.300	5	0	0.500	3.660
24	0.200	1.500	350	15.000	0.300	5	20	2.503	10.757
25	0.100	0.750	300	18.000	0.300	5	20	0.397	2.877
26	0.200	0.750	300	18.000	0.300	5	0	1.063	6.007
27	0.100	1.500	300	18.000	0.300	5	0	0.367	2.007
28	0.200	1.500	300	18.000	0.300	5	20	2.783	15.330
29	0.100	0.750	350	18.000	0.300	5	0	0.763	4.217
30	0.200	0.750	350	18.000	0.300	5	20	1.437	7.253
31	0.100	1.500	350	18.000	0.300	5	20	0.383	3.137
32	0.200	1.500	350	18.000	0.300	5	0	2.960	11.610
33	0.100	0.750	300	15.000	0.000	15	0	0.803	4.007
34	0.200	0.750	300	15.000	0.000	15	20	2.030	7.213
35	0.100	1.500	300	15.000	0.000	15	20	0.537	4.583
36	0.200	1.500	300	15.000	0.000	15	0	2.110	9.117
37	0.100	0.750	350	15.000	0.000	15	20	0.920	4.480
38	0.200	0.750	350	15.000	0.000	15	0	1.743	7.157
39	0.100	1.500	350	15.000	0.000	15	0	0.290	2.043
40	0.200	1.500	350	15.000	0.000	15	20	0.943	4.460
41	0.100	0.750	300	18.000	0.000	15	20	0.513	2.973
(Part II)									
42	0.200	0.750	300	18.000	0.000	15	0	2.087	7.550
43	0.100	1.500	300	18.000	0.000	15	0	0.430	2.823
44	0.200	1.500	300	18.000	0.000	15	20	2.557	10.570
45	0.100	0.750	350	18.000	0.000	15	0	0.350	2.457
46	0.200	0.750	350	18.000	0.000	15	20	1.700	6.507
47	0.100	1.500	350	18.000	0.000	15	20	0.617	3.057
48	0.200	1.500	350	18.000	0.000	15	0	1.747	8.273

Table 3 (continued)

Run	fz	ap	vc	ae	z_1	z_2	z_3	Ra	Rt
49	0.100	0.750	300	15.000	0.300	15	20	0.823	4.690
50	0.200	0.750	300	15.000	0.300	15	0	3.007	11.787
51	0.100	1.500	300	15.000	0.300	15	0	0.643	5.230
52	0.200	1.500	300	15.000	0.300	15	20	2.937	9.870
53	0.100	0.750	350	15.000	0.300	15	0	0.803	4.997
54	0.200	0.750	350	15.000	0.300	15	20	2.220	9.797
55	0.100	1.500	350	15.000	0.300	15	20	0.463	2.793
56	0.200	1.500	350	15.000	0.300	15	0	2.203	9.823
57	0.100	0.750	300	18.000	0.300	15	0	0.820	5.343
58	0.200	0.750	300	18.000	0.300	15	20	2.547	10.663
59	0.100	1.500	300	18.000	0.300	15	20	0.377	2.560
60	0.200	1.500	300	18.000	0.300	15	0	2.193	8.853
61	0.100	0.750	350	18.000	0.300	15	20	0.637	4.050
62	0.200	0.750	350	18.000	0.300	15	0	2.247	9.590
63	0.100	1.500	350	18.000	0.300	15	0	0.483	3.400
64	0.200	1.500	350	18.000	0.300	15	20	2.887	11.327
65	0.010	1.130	325	16.500	0.150	10	10	0.100	0.820
66	0.290	1.130	325	16.500	0.150	10	10	2.440	10.760
67	0.150	0.060	325	16.500	0.150	10	10	0.350	1.910
68	0.150	2.190	325	16.500	0.150	10	10	1.573	6.817
69	0.150	1.130	254	16.500	0.150	10	10	0.650	5.257
70	0.150	1.130	396	16.500	0.150	10	10	0.440	3.413
71	0.150	1.130	325	12.260	0.150	10	10	0.390	3.383
72	0.150	1.130	325	20.740	0.150	10	10	1.183	6.230
73	0.150	1.130	325	16.500	0.150	10	10	0.343	2.990
74	0.150	1.130	325	16.500	0.150	10	10	0.540	3.283
75	0.150	1.130	325	16.500	0.150	10	10	0.680	4.083
76	0.150	1.130	325	16.500	0.150	10	10	0.520	3.247
77	0.150	1.130	325	16.500	0.150	10	10	0.540	4.090
78	0.150	1.130	325	16.500	0.150	10	10	0.323	2.993
79	0.150	1.130	325	16.500	0.150	10	10	0.527	4.990
80	0.150	1.130	325	16.500	0.150	10	10	0.607	3.453
81	0.150	1.130	325	16.500	0.150	10	10	0.697	4.970
82	0.150	1.130	325	16.500	0.150	10	10	0.430	2.863

$$\sigma^2[\mathrm{Ra}(\mathbf{x})] = (0.102 + 0.048x_1 + 0.013x_2 + 0.020x_3 - 0.052x_4)^2 + (0.002 - 0.858x_1 - 0.073x_2 - 0.034x_3 - 0.013x_4)^2 + (0.005 + 0.042x_1 - 0.012x_2 - 0.041x_3 - 0.025x_4)^2 + \underbrace{0.990}_{\mathrm{MSE(Ra)}} \tag{9}$$

$$E_z[\mathrm{Rt}(\mathbf{x},\mathbf{z})] = 4.719 + 3.170x_1 + 0.251x_2 - 0.261x_3 + 0.046x_4 + 1.039x_1^2 + 0.176x_2^2 + 0.173x_4^2 + 0.498x_1x_2 - 0.225x_1x_3 + 0.233x_1x_4 - 0.020x_2x_3 + 0.164x_2x_4 + 0.181x_3x_4 \tag{10}$$

$$V_z[\mathrm{Rt}(\mathbf{x},\mathbf{z})] = \left[\frac{\partial \mathrm{Rt}(\mathbf{x},\mathbf{z})}{\partial z_1}\right]^2 + \left[\frac{\partial \mathrm{Rt}(\mathbf{x},\mathbf{z})}{\partial z_2}\right]^2 + \left[\frac{\partial \mathrm{Rt}(\mathbf{x},\mathbf{z})}{\partial z_3}\right]^2 + \sigma^2 \tag{11}$$

$$\sigma^2[\mathrm{Rt}(\mathbf{x})] = (0.877 + 0.311x_1 - 0870x_2 + 0.128x_3 - 0.158x_4)^2 + (0.040 - 0.291x_1 - 0.210x_2 - 0.109x_3 - 0.016x_4)^2 + (-0.049 + 0.188x_1 - 0.127x_2 + 0.042x_3 + 0.157x_4)^2 + \underbrace{0.910}_{\mathrm{MSE(Rt)}} \tag{12}$$

Equations (9) and (12) are composed of the square partial derivatives of y(**x,z**) and the MSE associated with each model accuracy. However, in the optimization, this term will not be minimized since it is independent of the controllable parameters. The graphs of Fig. 7 present the factorial plots for variance of Ra and Rt according to the models established in Eqs. (9) and (12). These graphs show how control parameters affect the instability of surface roughness, increasing its variance. It can be seen that for both Ra and Rt, the smallest values of variance occurs for low levels of feed per tooth (near to level −1, or 0.1 mm/tooth), small values for cutting speed (vc), and large values of radial depth of cut (ae). Larger values of axial depth of cut (ap) minimize the variance of Rt. Most of these levels, as is discussed below, are related to low levels of system vibration, thus indicating that it is possible to minimize the variance of surface roughness by minimizing the level of vibration.

Since the mean and variance equations of the two responses of interest are estimated, the proposed optimization procedure can be run. According to step x, an individual optimization of $E_z[\mathrm{Ra}(\mathbf{x},\mathbf{z})]$ and$E_z[\mathrm{Rt}(\mathbf{x},\mathbf{z})]$ is conducted, obtaining as the respective optimal values of ζ_{Ra}=0.230 μm and ζ_{Rt}=1.795 μm. These values are considered the targets and are utilized in composing each MSE(**x**) function. After individual optimization, one can obtain the values of $\mathrm{MSE}_T^{\max}(\mathbf{x})$ and $\mathrm{MSE}_i^I(\mathbf{x})$for both Ra and Rt. In both cases, the utopia points lead to the payoff matrix of Table 4.

Applying the MSE method and carrying out iteratively successive optimizations, we obtain the results found in Table 5.

The values presented in Table 5 were used to trace the Pareto frontiers for surface roughness (Ra × Rt) and MSE (MSE(Ra) × MSE(Rt)) as shown in Fig. 8. All points described in Fig. 8 are feasible; i.e., each point is capable of leading the process to an optimal condition—the lowest possible values for Ra and Rt with low variance—with different degrees of importance. The 21 setups described in Table 5 were obtained using a specific weight varying between 0 and 1, with increments of 5 %. In addition, each Pareto point falls within the region of interest, according to the constraint$\mathbf{x}^T\mathbf{x} \leq \alpha^2$**.** This may occur because there has been a convex

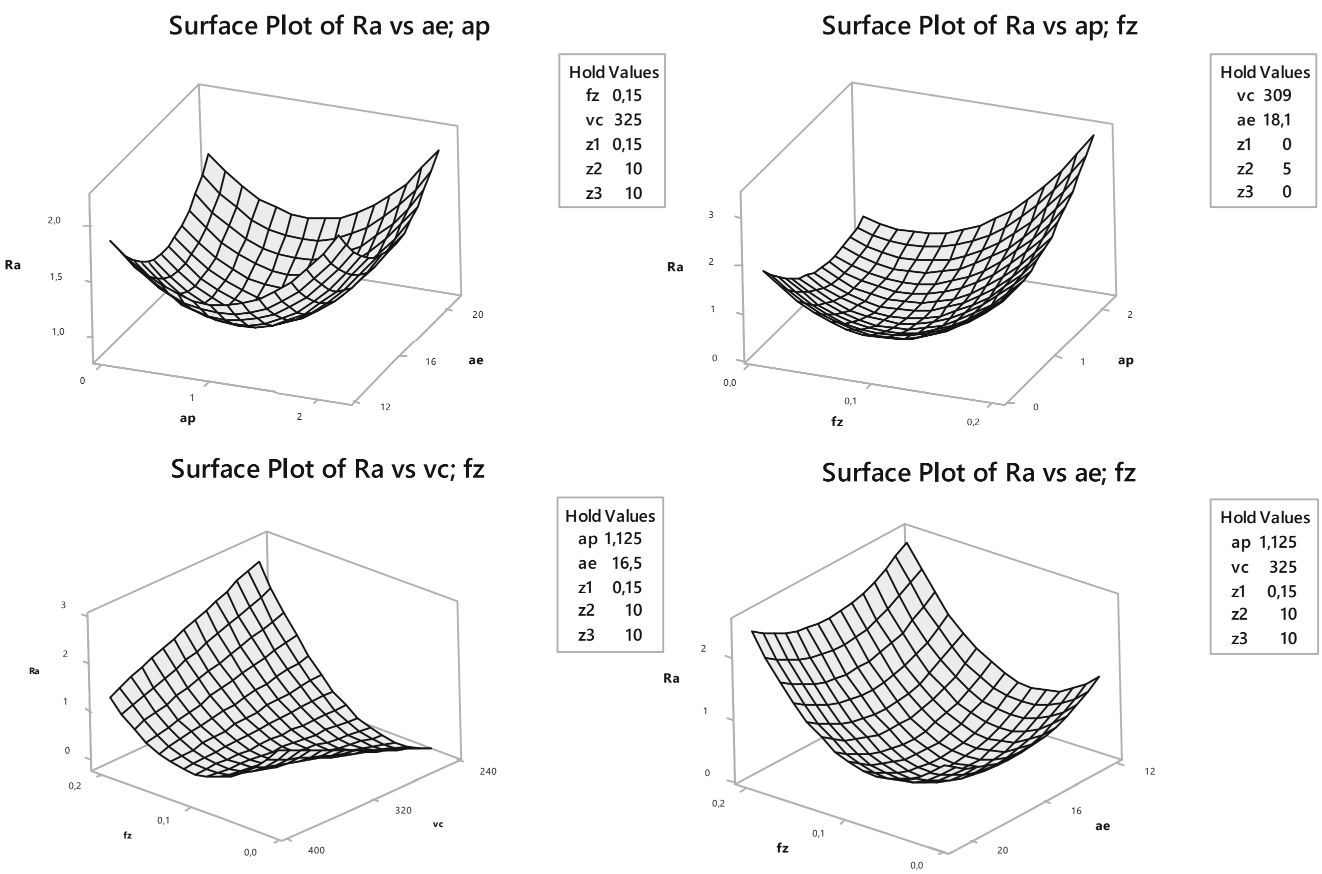

Fig. 3 Effect of interactions on average surface roughness (μm)

problem, with at least one convex MSE function. The method is mainly effective in the transition between optimization for the first and last individual applied weight with increments of 5 %.

Figures 8, 9, and 10 show the contour plots for surface roughness means and variances for an optimal obtained from Eq. (5) with $w=50$ %. It is clear this point is feasible and respects all the constraints.

5 Confirmation runs

The basic idea in robust design optimization concerns finding a setup of controllable factors that are insensitive to the actions of the uncontrollable factors. To test this claim, it is first necessary to determine an adequate sample size for testing the null hypothesis that the average values of Ra and Rt with the presence of noise factors are equal to the average value

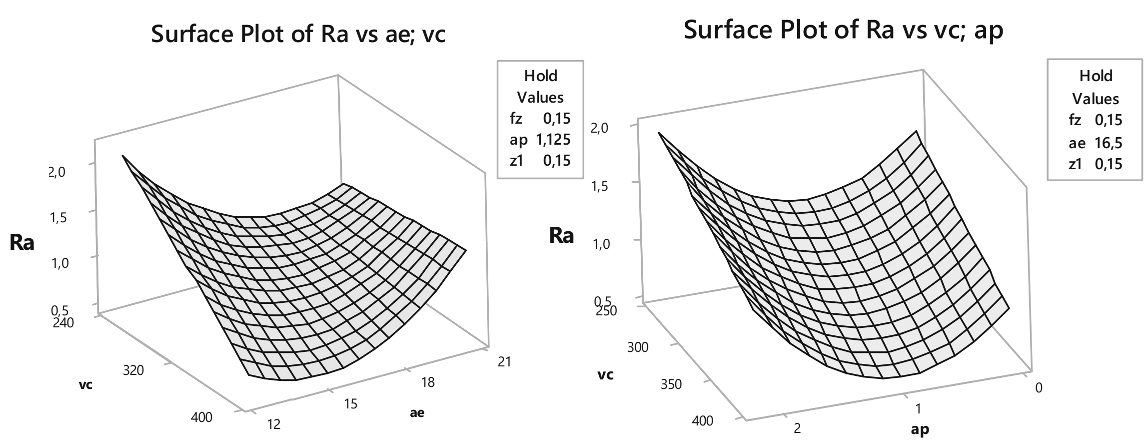

Fig. 4 Effect of interaction between vc versus ae and vc versus ap

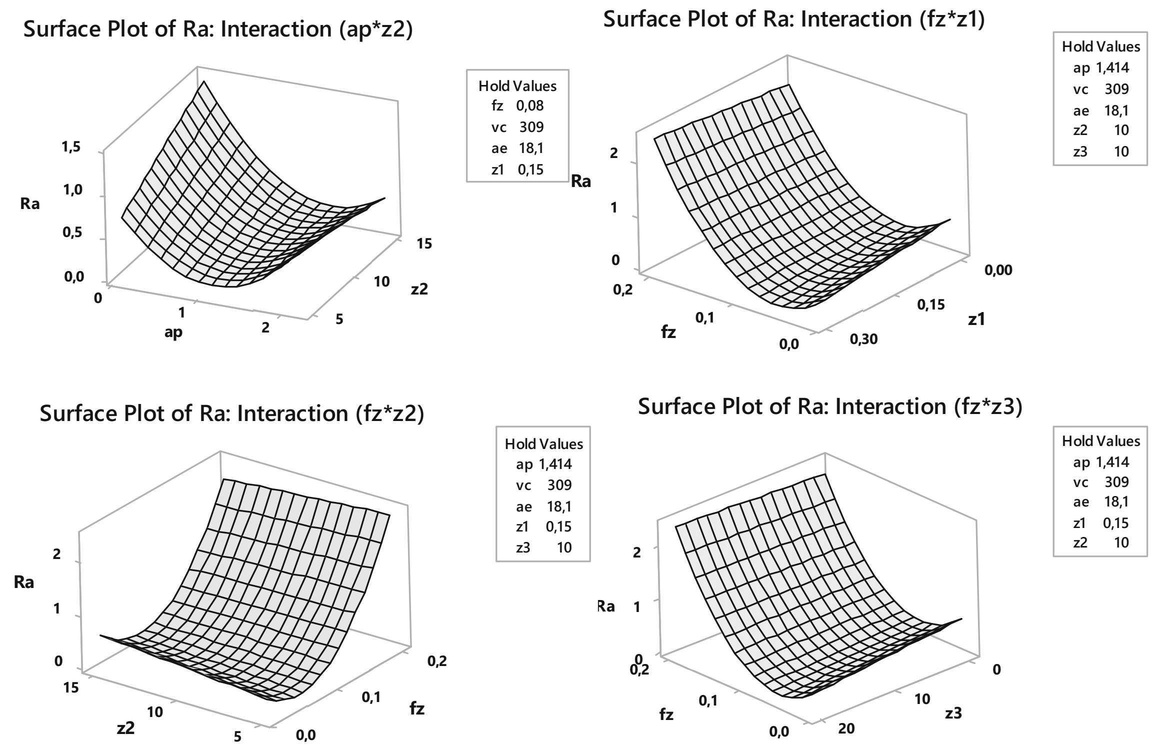

Fig. 5 Interactions between control and noise variables for Ra

without noise factors. If H0 is accepted, it means that, in this case, the noise factor effects were neutralized by robust setup. Selecting the optimal condition for w=50 % to test, $\mathbf{x}^{*}_{w=0.500}{}^{T} = [-1.373 \quad 0.771 \quad -0.645 \quad 1.051]$ or, in uncoded units, an end milling setup of $\mathbf{x}^{*}_{w=0.500}{}^{T} = [0.08\ \mathrm{mm/rev} \quad 1414\ \mathrm{mm} \quad 309\ \mathrm{m/min} \quad 18.1\ \mathrm{mm}]$, the optimal values of the solution vector keep the properties, summarized in Table 6.

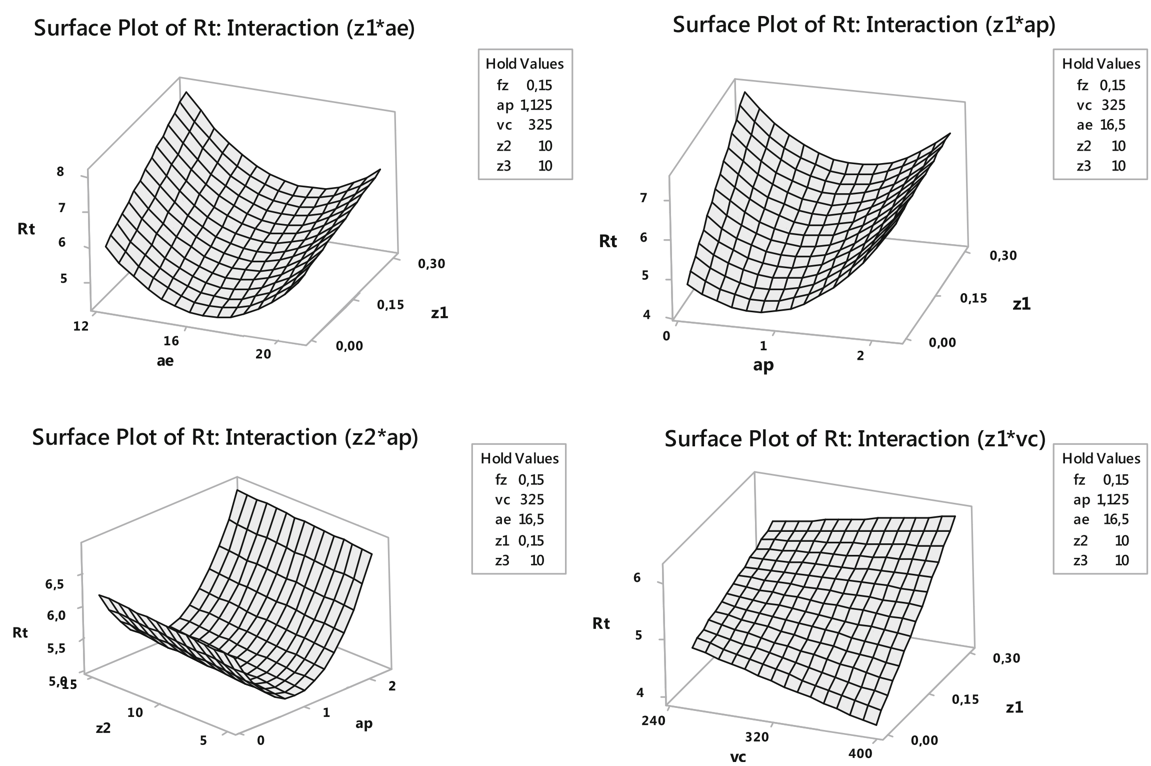

Fig. 6 Interactions between control and noise variables for Rt

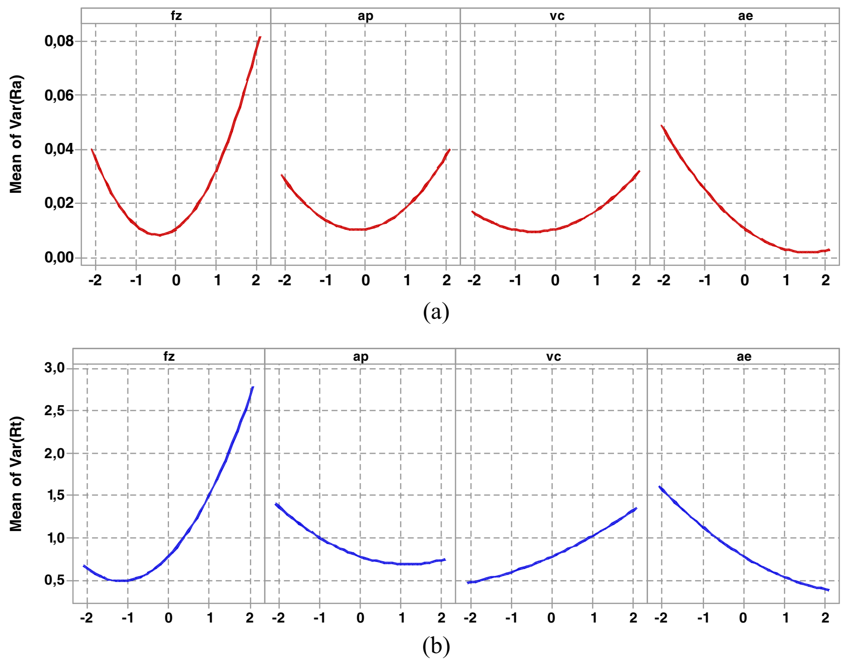

Fig. 7 Main effect plots for **a** Var (Ra) and **b** Var (Rt)

To test the effect of noise factors under the robust optimal condition for $w=50$ %, the L9 Taguchi design will be used to assess the influence of three noise factors with three levels. To determine the number of runs (or replicates) that should be carried out to test the neutralization of noise factor effects, the differences that should be detected with the test will also be considered. These differences were established based on the distance between the two anchor points of the Pareto frontier and the utopia and Nadir points for Ra and Rt, respectively. These values are denoted in Table 6 as "delta frontier" and "delta payoff." Based on these differences and the respective standard deviation values associated with the optimal point chosen on the frontier and assuming a power of 80 % and a significance level of 5 %, it is possible to obtain the power curves described in Fig. 11. According to these power curves, three replicates of the L9 Taguchi design are sufficient to detect the proposed differences with a power larger than 98 %. It can be noted that an L9 Taguchi design with three replicates is equivalent to the L27 design presented in Table 7. Such confirmation tests are shown in Table 7.

It is possible to note that the mean values for Ra and Rt obtained with the confirmation runs are very close to the predicted ones, with the same occurring for the MSE values. In addition, observing the results of ANOVA in Tables 8 and 9, it is possible to verify that none of the noise factors is significant (all P values >0.05), demonstrating that the setup is really robust to the presence of noise. It can also be seen that this occurs for the two segments of each three-factor levels of analysis. This means that with $\mathbf{x}^{*T}_{w=0.500} = [-1.373 \quad 0.771 \quad -0.645 \quad 1.051]$, the responses Ra and Rt do not change significantly in the presence of any combination of tool wear (z_1), lubricant flow rate (z_2), or concentration of lubricant (z_3). This is, for a variety of reasons, a crucial conclusion.

First, tool wear is a natural consequence of the physical process of removing material. In some respects, this is—since its occurrence is unavoidable—a noise factor. As the tool performance degrades with several machining passes, the optimal setup is thus incapable of ensuring that the surface roughness values remain the same. In the robust condition, however, tool usage in the process performance is assured for a long time. Second, since the lubricant is an oil-in-water emulsion, its concentration (z_2) can also be considered a noise factor, as its value can substantially change over the time.

Third, the slight importance of the lubricant flow rate (z_3) suggests that the end milling process of AISI 1045 could, without affecting the quality of the machined parts, be executed without any coolant or lubricant (or with scant amounts of them). It is well known that lubricants generally improve machining performance and that, without them, it is sometimes impossible to obtain an appropriate level of surface quality. For this reason, minimum quantity of lubrication (MQL), dry or semidry machining operations, and using very small amounts of lubricants are often desired. But, the combination of machined parts with a high level of surface quality along

Table 4 Payoff matrices

Payoff matrix for Ra and Rt		Payoff matrix for MSE_1 and MSE_2	
0.230	0.478	0.909	0.935
2.368	1.795	1.189	1.226

Table 5 Optimization results with weighted sums

Weights	x_1	x_2	x_3	x_4	Ra	Rt	Var Ra	Var Rt	MSE_1	MSE_2
0.000	−1.450	0.855	−0.347	1.022	0.446	1.977	0.910	1.184	0.957	1.217
0.050	−1.445	0.851	−0.369	1.026	0.442	1.978	0.910	1.184	0.955	1.217
0.100	−1.438	0.846	−0.392	1.030	0.438	1.979	0.910	1.184	0.953	1.218
0.150	−1.432	0.840	−0.417	1.034	0.433	1.979	0.910	1.184	0.951	1.218
0.200	−1.425	0.833	−0.444	1.038	0.429	1.980	0.910	1.184	0.949	1.218
0.250	−1.418	0.826	−0.473	1.041	0.423	1.981	0.910	1.184	0.947	1.219
0.300	−1.410	0.817	−0.503	1.045	0.418	1.982	0.910	1.185	0.945	1.220
0.350	−1.401	0.808	−0.536	1.047	0.412	1.983	0.909	1.185	0.943	1.221
0.400	−1.393	0.797	−0.570	1.049	0.406	1.985	0.909	1.186	0.940	1.222
0.450	−1.383	0.785	−0.606	1.051	0.399	1.987	0.909	1.187	0.938	1.224
0.500	−1.373	0.771	−0.645	1.051	0.392	1.989	0.909	1.189	0.935	1.226
0.550	−1.362	0.756	−0.685	1.050	0.384	1.991	0.909	1.191	0.933	1.229
0.600	−1.351	0.740	−0.728	1.048	0.376	1.994	0.909	1.193	0.931	1.232
0.650	−1.338	0.722	−0.773	1.044	0.368	1.998	0.909	1.195	0.928	1.236
0.700	−1.325	0.702	−0.821	1.038	0.359	2.003	0.909	1.198	0.926	1.241
0.750	−1.309	0.680	−0.873	1.030	0.349	2.009	0.909	1.202	0.923	1.247
0.800	−1.292	0.656	−0.930	1.018	0.339	2.019	0.909	1.206	0.921	1.256
0.850	−1.270	0.630	−0.994	1.001	0.327	2.032	0.909	1.210	0.919	1.267
0.900	−1.242	0.601	−1.070	0.976	0.314	2.055	0.909	1.216	0.916	1.283
0.950	−1.193	0.571	−1.170	0.939	0.299	2.105	0.909	1.221	0.914	1.317
1.000	−0.899	0.373	−0.607	0.594	0.281	2.635	0.905	1.263	0.908	1.968

with the use of low levels of lubricants depends on having an adequate level of machining parameters, something that cannot be achieved without an optimization strategy. It should be noted that, despite a very low lubricant flow rate or even in the absence of lubricant, surface roughness quality remains invariable. This represents a gain since there has been a rise in environmental concerns regarding the disposal of lubricant waste and its effects on human health. In fact, industries are obligated to review their technologies and procedures related to the consumption of these supplies.

Although the lubricant flow rate can be controlled, it is noteworthy that it is not uniformly applied to the tool part

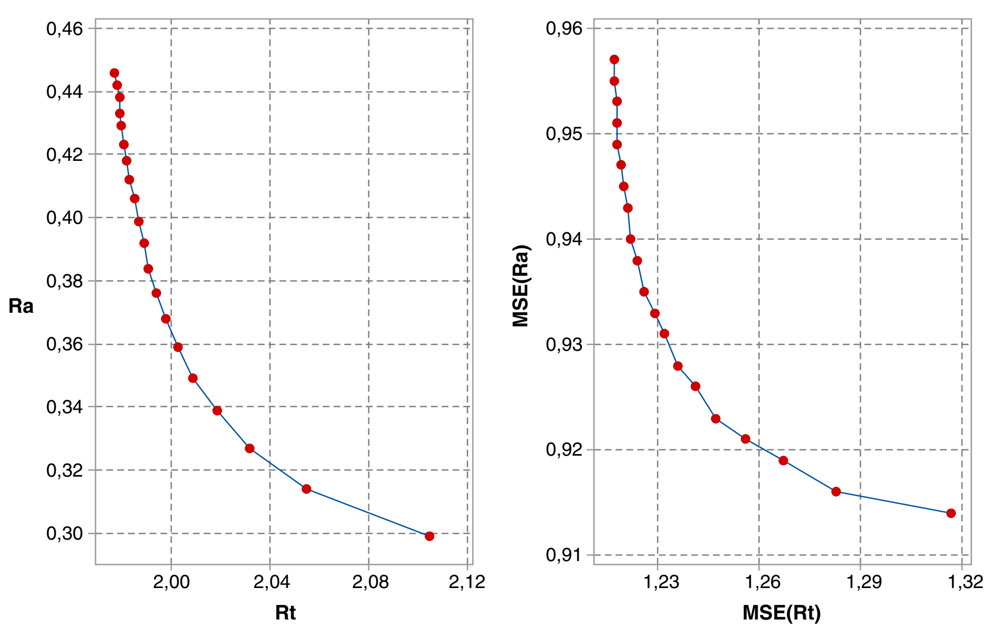

Fig. 8 Pareto frontiers for Ra versus Rt and MSE(Ra) versus MSE(Rt)

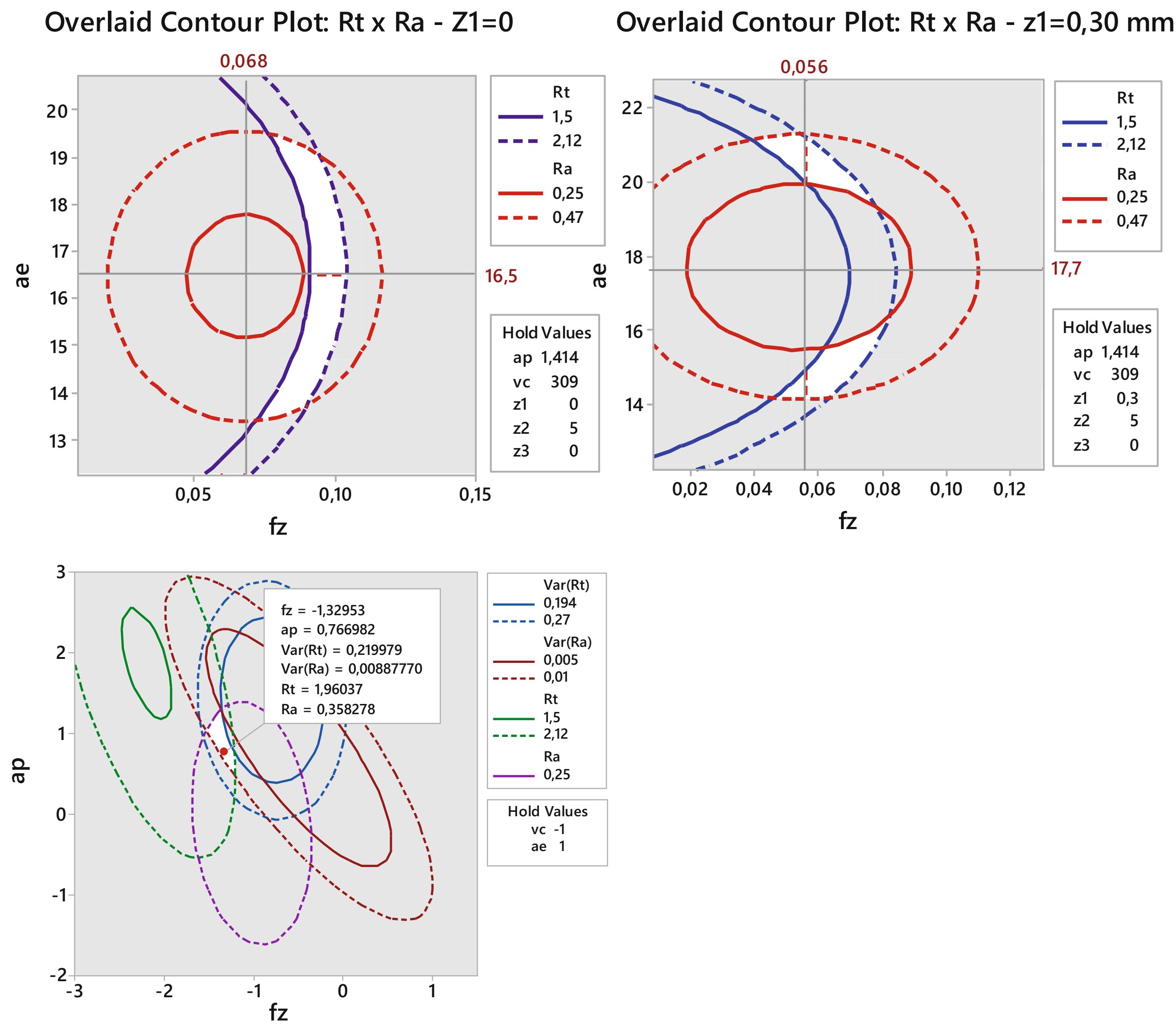

Fig. 9 Overlaid contour plots of mean and variance for w=50 % in Pareto frontiers

set, implying that some regions of a tool are not well cooled, promoting irregular or premature wear. In this sense then, the lubrication can be considered a noise factor.

Therefore, to ensure the quality of surfaces machined in an optimal setup, it is important to establish that an end milling process that is not vulnerable to the influence of variations in the lubricant flow rate, concentration, or tool wear is important. If these factors were to be neglected, it would be difficult to arrive at an optimal setup that could generate, over time, parts with the predicted optimal outcome. In other words, it is impossible to maintain an optimal surface roughness as a machining tool wears away or as the amount or concentration of lubrication changes. Hence, these facts are basically the difference between an optimal and a robust design, where all characteristics are controlled.

6 Discussion

The AISI 1045 steel end milling robust optimization led to a finishing setup capable of minimizing surface roughness Ra and Rt as well as minimizing their respective variances promoted by noise factors. The optimum set point of the process obtained by the optimization method [f=0.081 mm/dente; ap=1.414 mm; vc=309 m/min; ae=18 mm] was able to mitigate the effects of noise due to a combination of physical components of the milling process in question. There are some physical explanations for this phenomenon. For example, the lower feed per tooth (fz) minimizes the roughness of the part because it promotes a geometric effect of the inserts on the tips of peaks of the milled surface texture irregularities. The depth of cut (ap) obtained, near the level (+1), allows the mill to

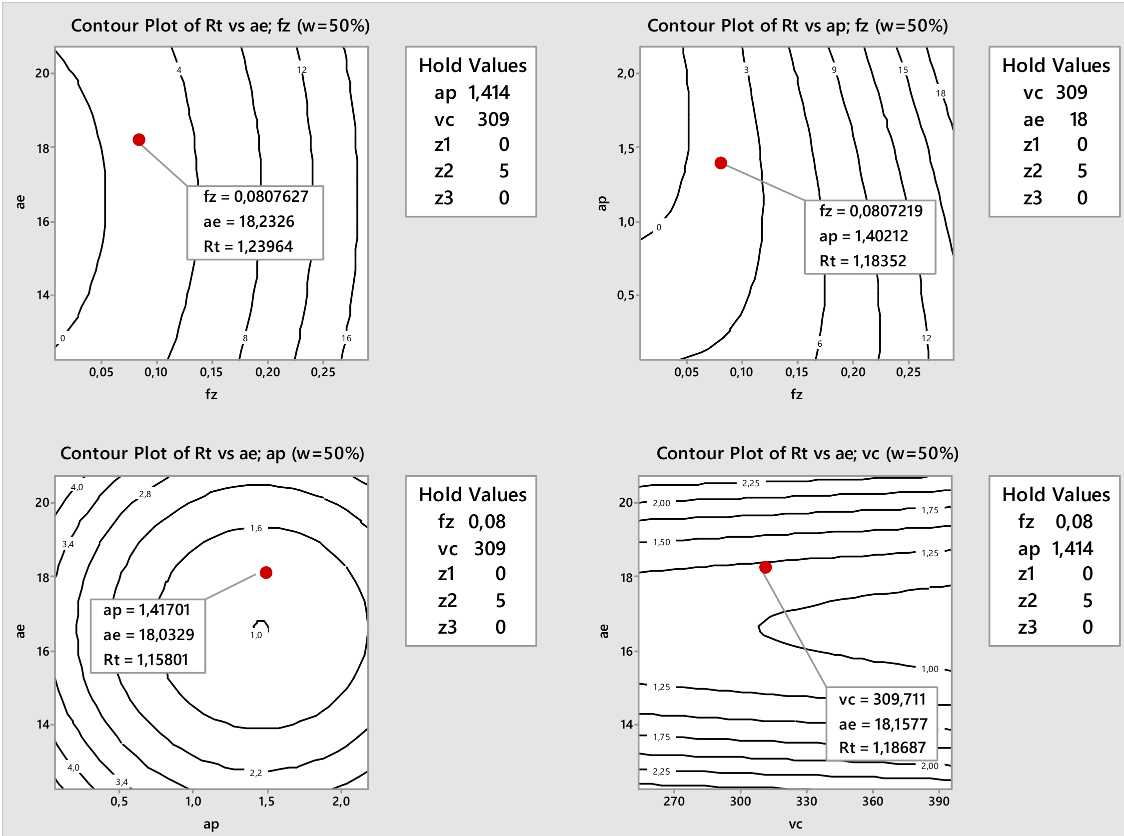

Fig. 10 Contour plots of Rt for w=50 %, with new tool (z_1=0.00 mm)

work with the main cutting edge and not just the nose radius (r=0.8 mm). This fact makes it easier to shear the workpiece material and prevents the formation of a lateral flow of the chip, which could harm the finish and increase the variance of roughness [28, 29]. The radial depth of cut (ae) obtained, near the level (+1) of DOE design, enables the mill to work with its center within the workpiece, with a ratio ae/Dc of around 70 %. This ratio of radial depth with cutting diameter (Dc) is considered optimal in terms of tool-workpiece engagement for asymmetrical cut end milling, which causes it to be less prone to the vibration process [28]. The smaller the vibration, the lower the roughness. The cutting speed (vc) obtained, near to level (−1), enables the mill to work on a smaller rotation. This makes it less likely that a vibration is brought to the rotation system of the machine tool and workpiece, since the machine used in the tests has a life longer than 10 years.

Table 6 Results referent to Pareto frontier point for a weight of w=50 %

$f(x)$	Mean	Utopia point	Delta payoff	Delta frontier	Variance	SD
Ra	0.392	0.230	0.248	0.165	0.009	0.096
Rt	1.989	1.795	0.573	0.658	0.199	0.446

The mitigating effects of flow (z_3) and cutting fluid concentration (z_2) on the part roughness can be explained by the milling operation conditions applied to parts of low hardness carbon steel (180 HB) being machined in typical finishing condition. In this condition, the specific power cut, which is given as the ratio between the active force and the rate of material removal, is relatively low, and thus, the thermal gradient generated in the cutting process was not so high. Thus, the variation of the concentration and flow rate of cutting fluid over the adopted levels did not influence the expected value or the variance of the workpiece roughness.

Last, the optimal setup promoted by RPD also neutralized the effect of the flank tool wear (z_1) over the surface roughness. When employing a new cutting edge, it is possible to achieve a better shear material, with low cut forces. Low cut forces lead to low system vibration and, consequently, a low level of surface roughness. The vibrations on the cutting tool have a momentous influence for the surface quality of the workpiece with respect to surface profile and roughness [4]. The results of Chen et al. [4] showed that the effects of feed rate and cutting depth provide a reinforcement of the overall vibration, giving rise to an unstable cutting process and, as a result, the worst machined surface. They also claimed that spindle speed and tool holder type affected the stability of cutting tooltip during the cutting process. With a worn-out

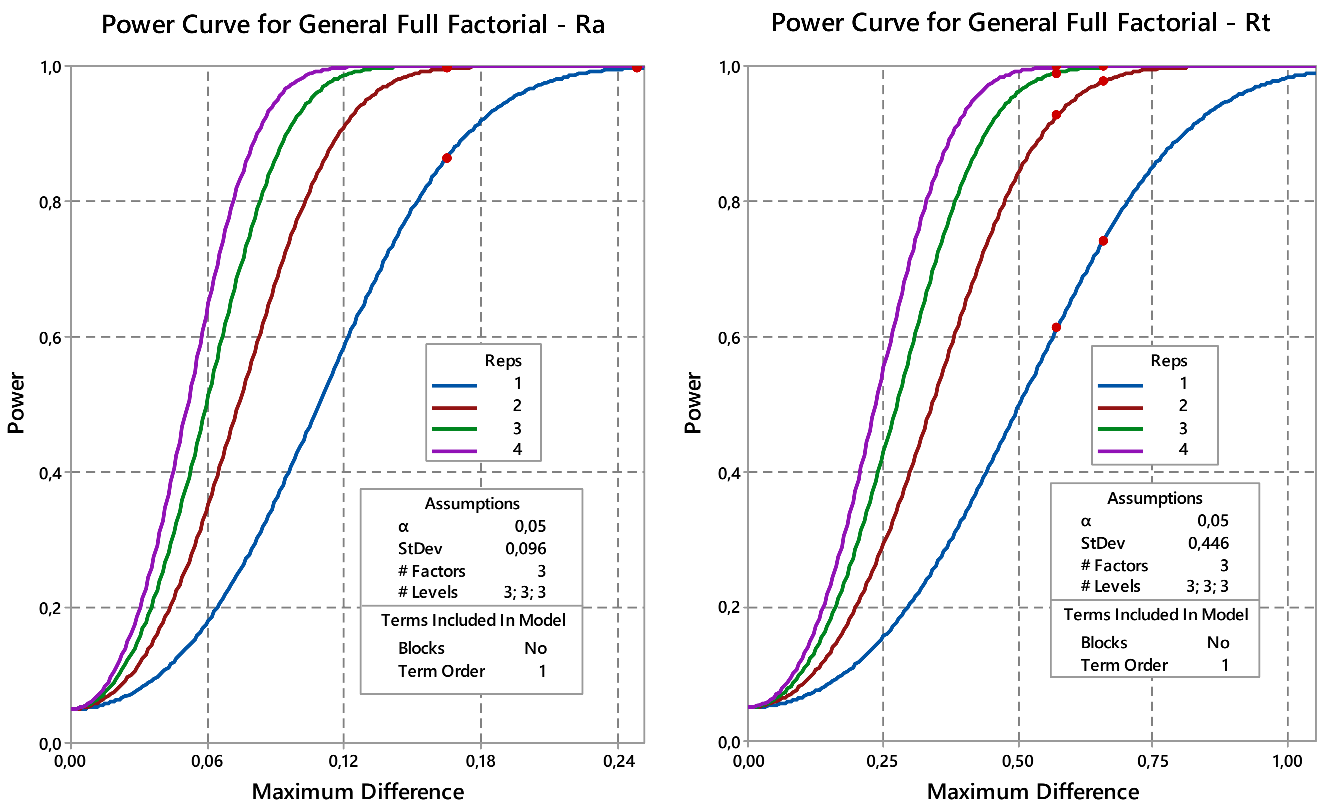

Fig. 11 Power and sample size calculation for confirmation runs

tool, the opposite effect occurs; however, the wear of secondary mill tool cutting edge generates a plane phase between the mill and the workpiece. This plane phase has a finishing effect, eliminating most of the roughness peaks during the operation and, in this way, reducing the surface roughness and respective variation [28].

7 Conclusions

This paper has reported the successful use of robust parameter optimization in the AISI 1045 end milling process using carbide inserts coated with titanium nitride (TIN). Here, RPD was capable of reducing the amount of system vibration during the machining process. In general, the lower the vibration level, the better the part finishing and the smaller the variance in the surface roughness profile. Among the several results obtained, the following are worth highlighting.

- RPD indicates that a lower feed per tooth (fz) is adequate to minimize the surface roughness because this allows the inserts to work properly, reducing the peaks of the irregularities on the milled surface.
- A large value of depth of cut (ap) allows the mill to work with the main cutting edge and not just the nose radius (r= 0.8 mm). This fact makes it easier to shear the workpiece material and prevents the formation of the chip's lateral flow, which could harm the finish and increase the variance of roughness.
- A large radial depth of cut (ae) obtained with RPD enables the mill to work with its center within the workpiece, reducing the vibration.
- The optimal setup produced an ae/Dc ratio of approximately 70 %. This ratio of radial depth with cutting diameter (Dc) is considered optimal because it also reduces the process vibration. RPD led to a small value of cutting speed (vc=309 m/min). This speed enables the mill to work on a smaller rotation, making an increase in vibration less likely.
- The optimal values of the Pareto frontier suggested a small power cut, which in turn is responsible for a low thermal gradient generated in the cutting process. Thus, the variation of the concentration and flow rate of cutting fluid over the adopted levels influenced neither the expected value nor the variance of the workpiece roughness.
- The method proves that the process may be extremely clean since it requires no refrigerant fluid.
- The optimal setup promoted by RPD also neutralized the effect of the flank tool wear (z_1) over the surface roughness because the balanced phenomena occurred with new and worn milling tools.

Table 7 L9 Taguchi design with three replicates (w=50 %)

z_1	z_2	z_3	Ra1	Ra2	Ra3	Mean	Rt1	Rt2	Rt3	Mean
0	5	0	0.43	0.39	0.40	0.407	2.23	2.16	1.76	2.050
0	5	0	0.46	0.35	0.37	0.393	2.83	2.57	2.72	2.707
0	5	0	0.51	0.35	0.46	0.440	2.56	3.20	2.72	2.827
0	10	10	0.36	0.48	0.39	0.410	2.02	2.44	2.66	2.373
0	10	10	0.43	0.37	0.54	0.447	2.35	2.28	2.12	2.250
0	10	10	0.34	0.37	0.35	0.353	2.24	1.90	2.34	2.160
0	15	20	0.38	0.38	0.47	0.410	1.81	2.13	2.86	2.267
0	15	20	0.38	0.43	0.33	0.380	1.50	2.46	2.17	2.043
0	15	20	0.35	0.43	0.51	0.430	2.46	2.86	2.87	2.730
15	5	10	0.41	0.55	0.37	0.443	2.63	2.37	2.52	2.507
15	5	10	0.34	0.26	0.27	0.290	2.11	2.14	2.14	2.130
15	5	10	0.54	0.50	0.40	0.480	2.00	2.54	1.98	2.173
15	10	20	0.31	0.40	0.51	0.407	2.22	2.28	2.57	2.357
15	10	20	0.35	0.31	0.39	0.350	2.12	1.32	2.29	1.910
15	10	20	0.45	0.46	0.52	0.477	2.28	2.73	2.98	2.663
15	15	0	0.40	0.40	0.39	0.397	2.35	2.38	2.21	2.313
15	15	0	0.47	0.36	0.46	0.430	3.16	2.38	3.05	2.863
15	15	0	0.40	0.45	0.33	0.393	3.12	2.61	2.23	2.653
30	5	20	0.28	0.35	0.41	0.347	2.53	2.19	2.77	2.497
30	5	20	0.32	0.32	0.46	0.367	1.39	2.23	2.40	2.007
30	5	20	0.36	0.27	0.28	0.303	2.22	1.71	1.54	1.823
30	10	0	0.36	0.48	0.39	0.410	2.02	2.44	2.66	2.373
30	10	0	0.43	0.37	0.54	0.447	2.35	2.28	2.12	2.250
30	10	0	0.34	0.37	0.35	0.353	2.24	1.90	2.34	2.160
30	15	10	0.39	0.45	0.36	0.400	2.52	2.38	2.28	2.393
30	15	10	0.38	0.32	0.37	0.357	2.32	2.46	2.19	2.323
30	15	10	0.35	0.46	0.42	0.410	1.82	1.83	2.53	2.060
Mean						0.403	Mean			2.362
Predicted value						0.398	Predicted value			1.795
Variance						0.001	Variance			0.051
MSE						0.931	MSE			1.361
Predicted MSE						0.938	Predicted MSE			1.226

- New cutting edges promote better shear material with low cut forces. Low cut forces lead to low system vibration and, consequently, a low level of surface roughness.

Table 8 ANOVA for L9 Taguchi design (noise factors) for Ra

Term	Coefficient	SE coefficient	T	P value
Constant	0.403	0.010	38.835	0.001
z_1 (0–15)	0.022	0.015	1.513	0.269
z_1 (15–30)	0.004	0.015	0.277	0.808
z_2 (5–10)	−0.005	0.015	−0.353	0.758
z_2 (10–15)	0.003	0.015	0.177	0.876
z_3 (0–10)	0.017	0.015	1.160	0.366
z_3 (10–20)	−0.004	0.015	−0.303	0.791

Table 9 ANOVA for L9 Taguchi design (noise factors) for Rt

Term	Coefficient	SE coefficient	T	P value
Constant	2.362	0.061	39.004	0.001
z_1 (0–15)	−0.080	0.086	−0.932	0.450
z_1 (15–30)	−0.029	0.086	−0.342	0.765
z_2 (5–10)	−0.060	0.086	−0.699	0.557
z_2 (10–15)	−0.109	0.086	−1.276	0.330
z_3 (0–10)	0.065	0.086	0.755	0.529
z_3 (10–20)	0.117	0.086	1.365	0.306

- The wear of secondary tool cutting edge generates a plane phase between the mill and the workpiece, eliminating most of the roughness peaks during the operation and, in this way, reducing the surface roughness and respective variation.
- From a mathematical perspective, the statistical models developed for responses of interest are characterized as expressions of great reliability, with high values of R^2 adj.
- The Pareto frontier presented 21 feasible solutions that led the process to a range of average roughness (Ra) between 0.25 and 0.47 μm depending on the weight chosen and range of 1.50 and 2.12 μm for Rt.
- These 21 setups also allowed for the minimization of variance of both Ra and Rt, with ranges [0.005; 0.010] and [0.194; 0.270], respectively.
- For w=50 %, the optimal setup is [f=0.081 mm/tooth; ap=1.414 mm; vc=309 m/min; ae=18 mm], a setup that was able to mitigate the effects of noise due to a combination of physical components of the milling process in question.
- The overlaid contour plots show that the feasible region is very narrow, showing the finding of robust solutions adequate for the process to be no trivial task.
- The statistical analysis of confirmation runs showed that the noise factors are neutralized, since all P values are less than 5 %. It was thus really possible, as the theory generally indicates, to make the end milling process insensitive to the influence of noise factors.

Acknowledgments The authors would like to express their gratitude to CNPq, CAPES, and FAPEMIG for their support in this research.

References

1. Öktem H (2009) An integrated study of surface roughness for modelling and optimization of cutting parameters during end milling operation. Int J Adv Manuf Technol 43(9):852–861
2. Routara BC, Bandyopadhyay A, Sahoo P (2009) Roughness modeling and optimization in CNC end milling using response

surface method: effect of workpiece material variation. Int J Adv Manuf Technol 40(11-12):1166–1180
3. Feng CX, Wang X (2002) Development of empirical models of surface roughness prediction in finish turning. Int J Adv Manuf Technol 20:348–356
4. Chen CC, Liu NM, Chiang KT, Chen HL (2012) Experimental investigation of tool vibration and surface roughness in the precision end-milling process using the singular spectrum analysis. Int J Adv Manuf Technol 63:797–815
5. Chakguy P, Siwaporn K, Pisal Y (2009) Optimal cutting condition determination for desired surface roughness in end milling. Int J Adv Manuf Technol 41:440–451
6. Adem KAM, Fales R, El-Gizawy AS (2015) Identification of cutting force coefficients for the linear and nonlinear force models in end milling process using average forces and optimization technique methods. Int J Adv Manuf Technol. doi:10.1007/s00170-015-6935-3
7. Alrashdan A, Bataineh O, Shbool M (2014) Multi-criteria end milling parameters optimization of AISI D2 steel using genetic algorithm. Int J Adv Manuf Technol 73:1201–1212
8. Bouzakis KD, Aichouhi P, Efstathiou K (2003) Determination of the chip geometry, cutting force and roughness in free form surface finishing milling, with ball end tools. Int J Mach Tools Manuf 43:499–514
9. Vining GG, Myers RH (1990) Combining Taguchi and response surface philosophies: a dual response approach. J Qual Technol 22:38–45
10. Box GEP, Jones S (1992) Design products that are robust to environment. Total Qual Manag 3(3):265–282
11. Kovach J, Cho BR (2008) Constrained robust design experiments and optimization with the consideration of uncontrollable factors. Int J Adv Manuf Technol 38:7–18
12. Shaibu AB, Cho BR (2009) Another view of dual response surface modeling and optimization in robust parameter design. Int J Adv Manuf Technol 41:631–641
13. Montgomery DC (2009) Design and analysis of experiments, 7th edn. Wiley, New York
14. Myers RH, Montgomery DC (2002) Response surface methodology: process and product optimization using designed experiments, 2nd edn. Wiley, New York
15. Del Castillo E, Montgomery DC (1993) A nonlinear programming solution to the dual response problem. J Qual Technol 25:199–204
16. Kim KJ, Lin DKJ (2006) Optimization of multiple responses considering both location and dispersion effects. Eur J Oper Res 169:133–145
17. Del Castillo E, Fan SK, Semple J (1999) Optimization of dual response systems: a comprehensive procedure for degenerate and non-degenerate problems. Eur J Oper Res 112:174–186
18. Ardakani MK, Noorossana R (2008) A new optimization criterion for robust parameter design—the case of target is best. Int J Adv Manuf Technol 38:851–859
19. Govindaluri SM, Cho BR (2007) Robust design modeling with correlated quality characteristics using a multi-criteria decision framework. Int J Adv Manuf Technol 32:423–433
20. Köksoy O, Yalcinoz T (2006) Mean square error criteria to multiresponse process optimization by a new genetic algorithm. Appl Math Comput 175(2):1657–1674
21. Köksoy O, Doganaksoy T (2003) Joint optimization of mean and standard deviation using response surface methods. J Qual Technol 35(3):239–252
22. Paiva AP, Campos PH, Ferreira JR, Lopes LGD, Paiva EJ, Balestrassi PP (2012) A multivariate robust parameter design approach for optimization of AISI 52100 hardened steel turning with wiper mixed ceramic tool. J Refract Met Hard Mater 30:152–163
23. Shin SS, Samanlioglu F, Cho BR, Wieceki MM (2011) Computing trade-offs in robust design: perspectives of the mean squared error. Comput Ind Eng 60:248–255
24. Shin SS, Cho BR (2005) Bias-specified robust design optimization and its analytical solutions. Comput Ind Eng 48:129–140
25. Tang LC, Xu K (2002) A unified approach for dual response surface optimization. J Qual Technol 34:437–447
26. Martínez M, García-Neto S, Sanchis J, Blasco X (2009) Genetic algorithms optimization for normalized normal constraint method under Pareto construction. Adv Eng Softw 40:260–267
27. Utyuzhnikov SV, Fantini P, Guenov MD (2009) A method for generating a well-distributed Pareto set in nonlinear multi-objective optimization. J Comput Appl Math 223:820–841
28. Sandvik-Coromant (2010) Metals machining technology. Technical Manual. Sandviken, Sweden
29. Trent EM, Wright PK (2000) Metal Cutting, 4th edn. Butterworth-Heinemann, USA